JOURNAL OF APPLIED ELECTROCHEMISTRY **27** (1997) 227–234

A mixture design approach to thermally prepared Ir–Pt–Au ternary electrodes for oxygen reduction in alkaline solution

Y. -J. LI, C. -C. CHANG, T. -C. WEN*

Department of Chemical Engineering, National Cheng Kung University, Tainan, Taiwan 70101, Peoples Republic of China

Received 19 December 1995; revised 2 July 1996

Thermally prepared ternary Ir–Pt–Au electrodes were investigated experimentally over their entire compositional range using the mixture design method. The results, involving voltammetric charges from electrode redox (q^*), oxygen reduction current densities (i), and their correspondingly electrocatalytic activities (i/q^*), are examined through regression models and response surface contour plots. Using mixture experimental design, the empirical models are fitted and plotted as contour diagrams which facilitate comparisons with experimental trends noted by other investigators and reveal the synergistic/antagonistic effects between the mixed oxides. The material characterization was performed by X-ray diffraction (XRD), X-ray photoelectron spectroscopy (XPS), and scanning electron microscopy (SEM) to assist in interpreting the electrocatalytic activity for oxygen reduction.

1. Introduction

Oxygen reduction is an industrially important electrochemical reaction which is applied to fuel cells [1], metal–air batteries [2], air depolarized cathodes [3], and the production of oxidant [4]. The applications of oxygen reduction are strongly dependent on the products produced, either OH^- or O_2H^-. Oxygen reduction is primarily considered to proceed through two pathways [5]: in one path, a four-electron reduction reaction without the formation of hydrogen peroxide; in the other, an initial reduction reaction to produce H_2O_2, then possibly electroreduced to OH^-. The pathway of oxygen reduction is actually dependent upon the nature of the electrode materials.

Iridium oxide (IrO_2) electrodes have been reported to be considerably more resistant to degradation in strong acid [6], and IrO_2 electrodes correspondingly exhibit remarkable anodic activity/stability in both acidic [7] and basic [8] solutions for both chlorine and oxygen evolution. Recently, IrO_2 has been used as a cathode for hydrogen evolution in both acidic and basic solutions [9,10]. Moreover, an IrO_2 electrode exhibits a broad peak corresponding to the Ir(IV)/Ir(III) redox transition between 0.5 and 1.0 V vs RHE [11], which could indicate an electrocatalytic species for oxygen reduction [12]. In addition, IrO_2 is a suitable substrate as a matrix for other materials due to its high electrocatalytic activity and stability.

In general, platinum exhibits better activities for oxidation and hydrogenation reactions than other transition metals. These catalytic properties might be due to the presence of vacancies in the *d*-band orbitals. Synergistic effects for platinum group bimetallic catalysts have been reported for hydrogen oxidation in hydrogen-oxygen fuel cells [13] and for other heterogeneous catalytic reactions [14]. Oxygen reduction at pre-reduced platinum is primarily via a four electron pathway in both acidic and basic solutions, as reported by Vilambi and Tayler [15]. Accordingly, platinum is considered an active electrocatalyst for oxygen reduction. Platinum requires a minimum amount of material, and provides maximum activity and good long term stability. Thus, the most popular component of binary [16–18] and ternary [19, 20] electrodes for oxygen reduction is undoubtedly Pt metal.

Several researchers have reported that gold cathodes give i/E responses which show a two-step reduction of oxygen, and rotating-ring-disc electrode (RRDE) experiments have confirmed the efficient formation of hydrogen peroxide by gold cathodes in the first reduction step [21–26]. Recently, Baez and Pletcher [27] reported that gold coating on titanium prepared by thermal decomposition was stable and formed a very strong bond with the substrate. Therefore, to promote the long term stability of the coating layer, gold on titanium substrate is worth studying.

The above information stimulated us to investigate oxygen reduction on thermally prepared Ir–Pt–Au ternary electrodes in alkaline media. For binary electrodes, the traditional approach of plotting properties against composition curves has provided an effective way of determining the synergistic effects of the materials in question. For ternary electrodes, however, no efficient experimental strategy exists. A

* To whom correspondence should be addressed.

 © 1997 Chapman & Hall

traditional approach would require a considerable expenditure of time and materials in the study of a moderate number of test samples. Alternatively, a mixture design method can be used. Mixture design strategy is based on statistical analysis, where a limited number of experiments is used in order to study the multicomponent system. In this study, a forward stepwise regression procedure was employed to achieve a statistically significant regression equation. The regression model was then plotted as both a property-against-composition diagram and a contour diagram via a computer program, which facilitated straightforward interpretations of the properties of binary or ternary systems. The purpose of this work is to study the effects of varying the composition of Ir–Pt–Au in ternary electrodes for oxygen reduction. The voltammetric charge and electrocatalytic activities are also examined and discussed in the following text.

2. Experimental details

2.1. *Preparation of electrodes*

Electrodes with various compositions were prepared by thermal decomposition of the following precursors: $IrCl_3{\cdot}xH_2O$ (Johnson Matthey, 51.6% metal content), $H_2PtCl_6{\cdot}xH_2O$ (Johnson Matthey, 47.6% metal content), and $AuCl_3{\cdot}xH_2O$ (Johnson Matthey, 65% metal content). The precursors, in the appropriate molar ratios (refer to Table 1), were dissolved in isopropanol solution containing 10% by volume concentrated HCl, giving a 0.25 mol dm^{-3} total solution. The titanium supports were first degreased with soap and water, then etched for 1 h in a 6 M HCl solution at 80 to 90 °C. A particular Ir, Pt and Au coating was formed by baking the etched plate at 85 °C for several min after it was dipped in its respective coating solution. After drying, the support was heated under air flow at an annealing temperature of 400 °C for 10 min. The entire procedure was repeated six times, after which the support was heated at the annealing temperature for one hour. The amount of oxide (*ca.* 0.8–1.2 mg cm^{-2}) formed on the titanium substrates was determined by weight. After this procedure, the thermally prepared electrodes were then pretreated by 20 CVS sweeping from 0.4 to −1.0 V at 100 mV s^{-1}. After this pretreatment, the shapes of further CV sweeps did not significantly differ.

2.2. *Electrochemical characterization*

Electrochemical experiments were investigated by cyclic voltammetry and steady-state potentiostatic techniques. Voltammetry was performed by using a BAS-100B (Bioanalytic System, Inc. USA) in a three-electrode cell with an Ag/AgCl electrode (Argenthal, 3 mol dm^{-3} KCl, 0.207 V vs NHE at 25 °C) acting as reference and a platinum wire serving as counter electrode. A Luggin capillary, whose tip was set at a distance of approximately 1 mm from the surface of the working electrode, was used to minimize errors due to *iR* drop. Cyclic voltammetry was carried out between −1.0 to 0.6 V vs Ag/AgCl at 0.1 V s^{-1}. In the steady-state oxygen reduction experiments, the measurement of reduction current was carried by an HA-301 potentiostat/galvanostat system (Hokuto Denko Company, Japan) at a stirring rate of 1200 rpm. The electrode was maintained at the desired Tafel-region potential and the *i*/*t* relation was recorded. The current density obtained from this *i*/*t* correlation at $t = 3$ min is defined as the steady state current density (i) for oxygen reduction.

All solutions used in this work were prepared with ultrapure water (18 MΩ cm) produced by a reagent water system (Milli-Q SP, Japan). In addition, cyclic

Table 1. Design matrix and experimental results of Ir–Pt–Au ternary electrodes

Electrode	*Solution composition*					
	x_1 (*Ir*)	x_2 (*Pt*)	x_3 (*Au*)	q^* mC cm^{-2}	$i^\dagger$ μA cm^{-2}	$i^\dagger/q^*$ μA mC^{-1}
1	1	0	0	40.57	10.82	0.26
2	0	1	0	27.29	436.72	16.00
3	0	0	1	1.17	8.48	7.25
4	1/3	1/3	1/3	35.52	978.13	27.54
5	1/2	1/2	0	96.47	550.24	5.70
6	0	1/2	1/2	30.25	612.40	20.24
7	1/2	0	1/2	29.88	38.37	1.28
8	2/3	1/6	1/6	100.89	789.94	7.83
9	1/6	2/3	1/6	80.53	1079.00	13.40
10	1/6	1/6	2/3	49.53	782.93	15.81
11	3/4	1/4	0	132.03	883.58	6.69
12	1/4	3/4	0	115.97	1012.80	8.73
13	3/4	0	1/4	25.96	9.58	0.37
14	1/4	0	3/4	13.24	43.30	3.27
15	0	3/4	1/4	29.15	566.53	19.43
16	0	1/4	3/4	13.46	344.80	25.62

† Current density for oxygen reduction at −135 mV vs Ag/AgCl in 1 M KOH at 25 °C.

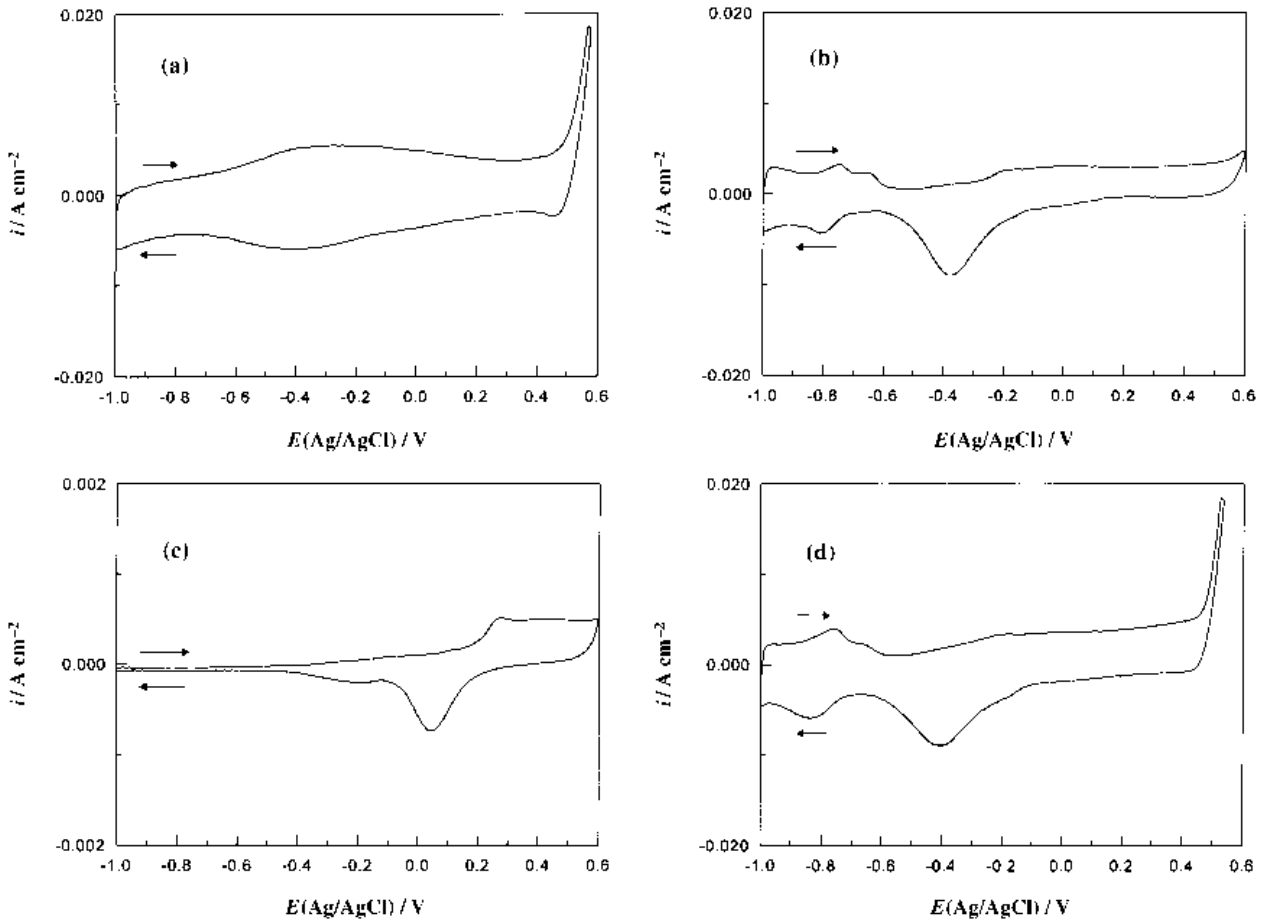

Fig. 1. Voltammetric response of (a) IrO_2, (b) Pt, (c) Au and (d) Ir–Pt–Au electrodes. The cyclic voltammograms were run in 1 mol dm^{-3} KOH with a scan rate of 0.1 V s^{-1}.

voltammetry investigations and oxygen reduction measurements were performed under purging nitrogen and oxygen, respectively, and all potentials are quoted against Ag/AgCl. Voltammetry and oxygen reduction measurements were carried out in 1 M KOH solution prepared from special low carbonate KOH pellets (Merck, GR). All measurements were maintained at 25 °C by means of a water thermostat (Haake D8 and G).

2.3. *Material characterization*

The surface morphology of various oxide electrodes was examined by scanning electron microscopy (SEM) (Jeol JSM 35 SEM). The X-ray photoelectron spectroscopy (XPS) were performed with ESCA 210 and Microlab 310D (VG Scientific Limited) spectrometers. XPS spectra employed MgK_α irradiation as the photon source. The crystalline structure was measured via X-ray diffraction analysis (XRD) (Rigaku D/MAX-*IIIV* X-ray diffractometer using a CuK_α source) at an angular speed of 4°(2θ) min^{-1}.

3. Results and discussion

3.1. *Voltammetric behaviour*

Cyclic voltammetry is recognized as being the most informative, real time method of oxide characterization. Accordingly, cyclic voltammograms of the prepared electrodes are useful for understanding the role of the corresponding redox in the interesting potential ranges on the whole. Thus, voltammetric responses of IrO_2 (no. 1), Pt (no. 2), Au (no. 3), and Ir-Pt-Au (no. 4) electrodes in 1M KOH at a scan rate of 100 mV s^{-1} are shown in Fig. 1(a),(b),(c) and (d) respectively. An examination of Fig. 1(a) reveals that the IrO_2 electrode (no. 1) possesses a broad peak corresponding to the Ir(IV)/Ir(III) redox transition between −0.5 and 0 V. This redox was reported as electrocatalytic species for oxygen reduction [12]. Fig. 1(b) shows the voltammetric behaviour of a Pt (No. 2) electrode. In the potential range between oxygen and hydrogen evolution, the oxidation and reduction behaviours are similar to those of pure platinum which agrees with previous work [28–30]. As for Au (no. 3, Fig. 1(c)), the CV response is not obvious due to its lesser activity in the potential range of interest, but the electrochemical behaviour of the thermally prepared Au electrode is similar to that of pure gold [31–33]. Fig. 1(d), the Ir–Pt–Au ternary electrode (no. 4), shows the combined CV responses of Ir, Pt and Au, including the redox transition and the shape of the curve. The hydrogen adsorption/desorption portion of the curve becomes obvious due to the domination of Pt behaviour, and the oxygen evolution starting potential of this ternary electrode, which is influenced by the addition of iridium oxide, is less

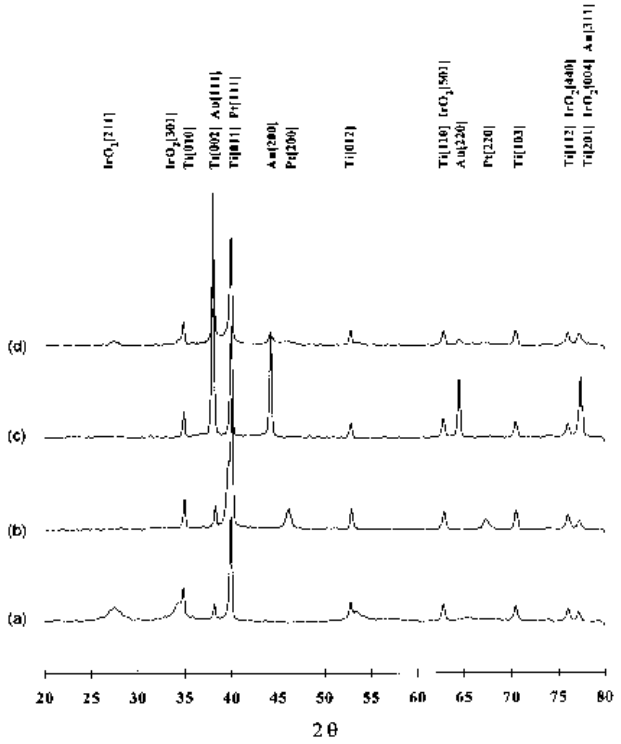

Fig. 2. The X-ray diffraction scan of (a) IrO_2, (b) Pt, (c) Au and (d) Ir–Pt–Au electrodes at angular speed of 4°(2θ) min^{-1}.

positive than that of the Pt electrode. In addition, the characteristics of gold do not obviously appear in the CV behaviour since the CV characteristics of gold are much smaller than those of Ir and Pt.

To confirm the information from our CVs, XRD and XPS spectra for Pt $4f_{7/2}$ were used to generate structural information for cross-checking the CV results. The XRD results of Ir, Pt, and Au, and Ir–Pt–Au electrodes are shown in Fig. 2(a), (b), (c) and (d), respectively. In Fig. 2(a), the visible peaks are definitely from crystalline planes of IrO_2 and Ti, revealing that IrO_2 was coated on titanium substrate. In Fig. 2(b) and (c), the coatings from the H_2PtCl_6 and $AuCl_3{\cdot}xH_2O$ solutions show pure Pt and Au peaks only, presumably due to these metals' reluctance to form oxides. These results are similar to those reported previously [28, 29]. Thermally prepared Pt/Ti was produced via thermal decomposition of H_2PtCl_6 by Comninellis and Vercesi [28], who reported that this preparation leads to PtO_x with $x \leq 0.18$. Thus, our assertion that the thermally prepared Pt after CV pretreatment leads to pure Pt behaviour is reasonable. As for Fig. 2(d), all peaks of IrO_2, Pt and Au appearing in the coating indicate that this electrode is coated with the metal state of both Pt and Au as well as the oxide state of Ir. Since the Pt [1 1 1] and Pt [2 0 0] peaks from our XRD results are not clear and, in fact, suggest no Pt in the sample, an XPS spectrum is used to confirm the presence of Pt on the electrode surface. Figure 3 shows the XPS spectrum of Pt $4f_{7/2}$ for an Ir–Pt–Au electrode. The analysis of the Pt $4f$ line confirms that Pt does exist in the sample [29]. The difference between XRD and XPS results thus indicates that Pt is present almost exclusively on the

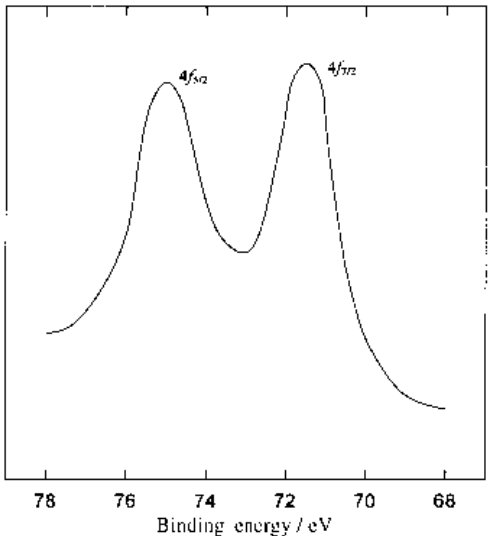

Fig. 3. XPS spectra of Pt $4f_{7/2}$ for Ir–Pt–Au electrode.

surface, the so-called surface enrichment phenomenon, as corroborated by previous papers [29, 34, 35]. Based on the above discussion, the combination of both XRD and XPS results definitely supports the information from our CV results.

3.2. *Voltammetric charge*

The voltammetric charge (q^*) has been reported as being directly proportional to the number of an electrode's electrochemically active surface sites [8, 36, 37]. Therefore, the voltammetric charge (q^*), on either the positive or negative sweeps in the potential region between hydrogen and oxygen evolutions, is assumed to represent the number of active surface sites on an electrode. In fact, it is dependent on (i) geometrical roughness, (ii) dispersion of active species and (iii) electronic structure of active species. Thus, both voltammetric behaviour and charge are thought to be effective indexes for categorizing the electrochemical properties of electrodes.

Ternary electrode q^* data were obtained by numerical integration within the aforementioned potential range (hydrogen evolution to oxygen evolution), with integration restricted to the range 0.4 to −0.6 V on the negative sweep, in order to avoid overestimation of the active sites due to oxygen evolution and to diminish the influence of hydrogen adsorption/desorption. The results are listed, together with the design matrix, in Table 1. Regression equation coefficients for the q^* approximation model were calculated from the experimental q^* values in Table 1 with the aid of appropriate formulae, and resulted in the following equation:

$$\underset{(12.47)}{q^* = 50.53x_1} + \underset{(12.47)}{38.38x_2} + \underset{(65.54)}{330.49x_1x_2} \quad (1)$$

where x_1 and x_2, respectively, represent the molar proportions of Ir and Pt in the coating solution. The numbers in the parentheses below the coefficients are their standard errors judged from error variance (s^2 =

mean square of error = 338.39). The detailed descriptions of the statistical meaning of regression equation coefficients can be found in our previous paper [8,38] or [39]. The analysis of q^* variance is presented in Table 2. The test statistics, F and R^2_{adj}, are defined as

$$F = \frac{MSR}{MSE}$$

$$R^2_{adj} = 1 - \frac{SSE/(N-P)}{SST/(N-1)}$$

where MSR is the mean square of regression, obtained via dividing the sum of squares of regression by the degree of freedom. MSE is the mean squares of error from the analysis of variance. If the calculated value of F is greater than that in the F table at a specified probability level (i.e., $F(P-1, v, 1-\alpha)$), then a 'statistically significant' regression model is obtained, where v is the degree of freedom of error and P is the number of parameters. R^2_{adj} is a measure of reduction in the estimate of the error variance due to the fitting of the model, $SSE/(N-P)$, relative to the estimate of the error variance based on fitting the simple model $y = \beta_0 + \varepsilon$ [39]. SSE and SST are the sum of the squares of error and sum of squares of total, respectively. N and P are the number of observations and parameters, respectively. R^2_{adj} is the adjusted correlation coefficient (R^2), with a value close to 1 meaning a perfect fit to the experimental data. These quantities are the criteria used in determining how well the model fits the data.

Regression Equation 1 was used in constructing the contour plot (Fig. 4) of voltammetric charge against Ir–Pt–Au precursor composition, which facilitates a straightforward examination of the dependence of q^* on the composition of both binary (Ir–Pt, Ir–Au and Pt–Au) and ternary (Ir–Pt–Au) oxide systems. From the statistical point of view, the magnitudes of the regression coefficients compared to their standard errors are used as a basis for judging statistical significance and for illustrating the relative effects of q^* on linear and nonlinear blending of synergistic and antagonistic effects in single, binary, and ternary systems. The contribution of Ir to the voltammetric charge is indicated by the coefficient associated with the x_1 term, which is 50.53. These data result from the broad peak corresponding to the Ir(IV)/Ir(III) redox transition. Similarly, the unitary effect of Pt on voltammetric charge is indicated by the coefficient associated with the x_2 term, which is 38.38. As for Au, the coefficient of unitary effect associated with the x_3 term is zero. Obviously the reason for the zero value of the contribution of Au to the voltammetric charge is its very low q^* value as compared to the q^* value of IrO_2 and Pt (see Table 1, electrode 1 and 2). The less active properties of gold may be due to the presence of completely filled d-orbitals [32]. As SEM photographs attest, the morphology of the Au electrode (Fig. 5(a)) is less cracked and more compact than that of IrO_2 (Fig. 5(b)) and Pt (Fig. 5(c)) electrodes, contributing to much smaller voltammetric charge. Accordingly, the effect of varying Au composition on the voltammetric charge is not significant and is therefore neglected in Equation 1. From a further examination of Fig. 4, voltammetric charge decreases with increasing Au content, being attributable to the lower activity of gold.

Table 2. Analysis of variance for the fit of q^* for Ir–Pt–Au ternary oxide electrodes

Source	*Sum of squares*	*Degrees of freedom*	*Mean square*	*F*
Model	62 245.12	3	20 748.37	61.32
Error	4399.05	13	338.39	
Total	66 644.17	16		

$R^2 = 0.9340$
$R^2_{\text{adj}} = 0.9238$.

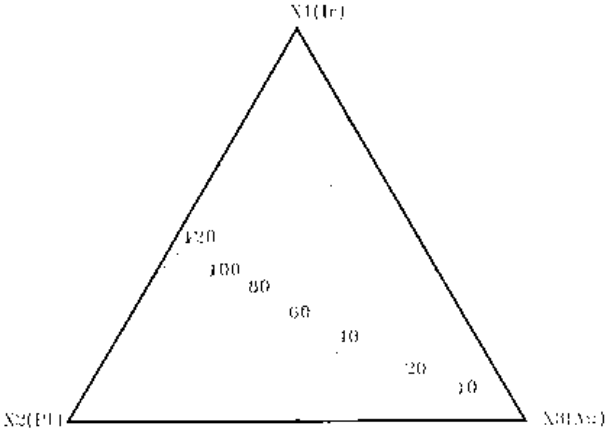

Fig. 4. A contour plot of voltammetric charge (mC cm^{-2}) against coating solution compositions for Ir–Pt–Au ternary oxide electrodes. Numbers associated with contour lines represent q^* results.

In Fig. 4, the maximum q^* (~ 120 mC cm^{-2}) occurs in the Ir–Pt binary system possessing 40 to 65% Ir content, which is about three times larger than those of unitary Pt and Ir electrodes. In addition, SEM photographs of Ir–Pt (Fig. 5(d)) show a more cracked surface than those of IrO_2 (Fig. 5(b)), Pt (Fig. 5(c)), and Au (Fig. 5(a)), which is one of the possible reasons for this electrode having the largest number of active surface sites. This can also be explained by the fact that Pt-dispersion on the IrO_2 matrix generates the high degree of nonstoichiometry of maximum q^* value IrO_2. It follows from the above discussion that IrO_2, as a matrix for other materials, might exhibit remarkable specific electrochemical behaviour. Consequently, modifying the Ir–Pt ratios may lead to the optimum voltammetric charge for Ir–Pt binary electrodes. From the statistical point of view, the synergistic effect indicated by the coefficient associated with the x_1x_2 term is larger than the unitary effects (x_1, x_2 and x_3), which increases the number and/or activity of the electrochemically active surface sites. This synergistic effect may be due to (i) the dispersal of platinum on the IrO_2 matrix, resulting in a larger active surface area (high q^* value) for Ir–Pt binary electrode, (ii) variation in surface roughness, and (iii)

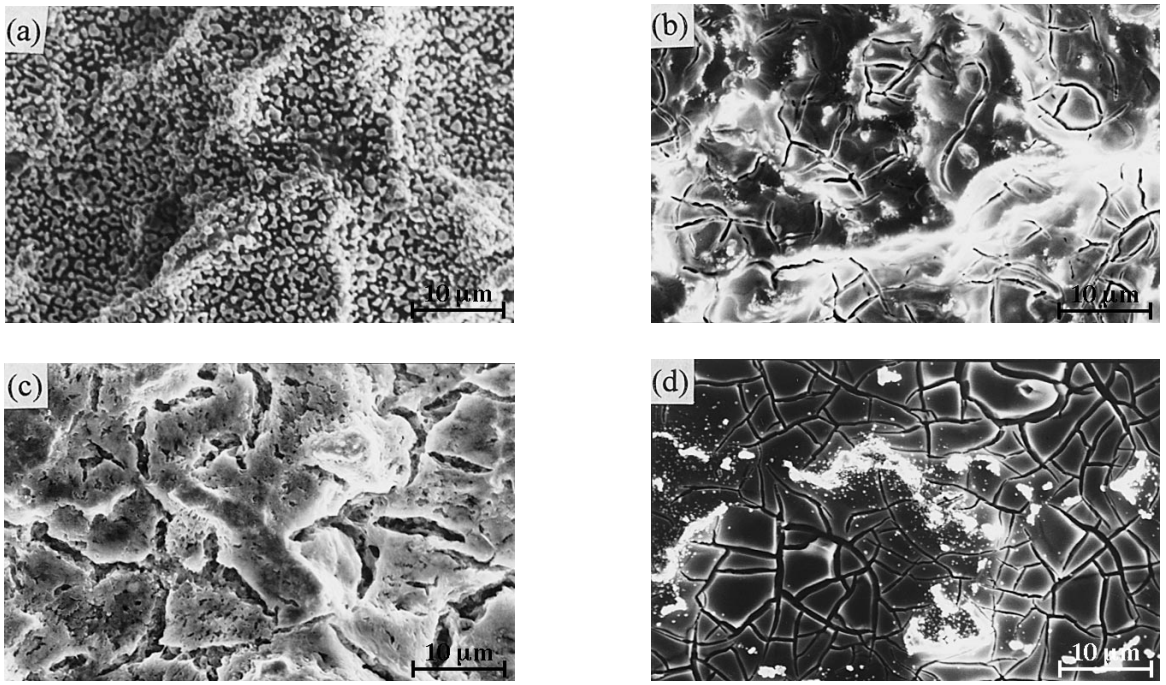

Fig. 5. SEM photographs of (a) Au, (b) IrO_2, (c) Pt, (d) Ir–Pt(50%–50%) binary electrodes.

a large number of defects on the mixed electrode. However, the real reasons responsible for this phenomenon are still unknown.

3.3. *Apparent electrochemical activity*

The electrochemical activities of the prepared electrodes were evaluated on the basis of their relative oxygen reduction current density at a constant electrode potential (−135 mV vs Ag/AgCl) and are listed together with the design matrix (electrode configuration) in Table 1. The regression equation for i, in Table 1, is of the following form:

$$\begin{aligned} i = {} & \underset{(139.07)}{451.834x_2} + \underset{(548.54)}{2670.70x_1x_2} + \underset{(548.54)}{1456.25x_2x_3} \\ & + \underset{(4037.08)}{14745x_1x_2x_3} \end{aligned} \tag{2}$$

The regression result with analysis of variance indicates that the regression model is statistically significant. In Equation 2, the only unitary effect is the coefficient of x_2 (i.e. Pt); in other words, Pt is an active catalyst for oxygen reduction. The synergistic effects are indicated by the coefficients associated with the x_1x_2, x_2x_3 and $x_1x_2x_3$ terms. Accordingly, not only Pt/Ir, but also Au, dominate the oxygen reduction currents. The contour plot of the apparent oxygen reduction current i relative to the Ir–Pt–Au ternary systems, as computed from Equation 2, is shown in Fig. 6. From an examination of Fig. 6, the reduction current reaches a maximum value of about 1200 μA cm^{-2} in Ir–Pt–Au ternary systems possessing 15–30% Au composition. Note that Ir–Au binary electrodes are lower than their Ir–Pt and Pt–Au counterparts. In addition, the reduction currents of unitary electrodes (Ir, Pt, Au) are also lower than those of binary electrodes (Ir–Pt, Pt–Au). In conclusion, the oxygen reduction current depends, not only on the unitary component effect, but also on the binary or ternary component effects. The above effects can be confirmed by the true catalytic results of the mixed components, which will be detailed in the following.

3.4. *Electrocatalytic activity*

To optimize the design of catalysts and identify the true catalytic effects of the mixed electrode materials, an investigation of the electrocatalytic activities of these materials, singularly and in groups, is essential and important. The electrocatalytic activity can be represented by i/q^*, which represents normalized activity, taking into account variations in active surface area (estimated by q^*) [38, 40]. In general, q^* is pro-

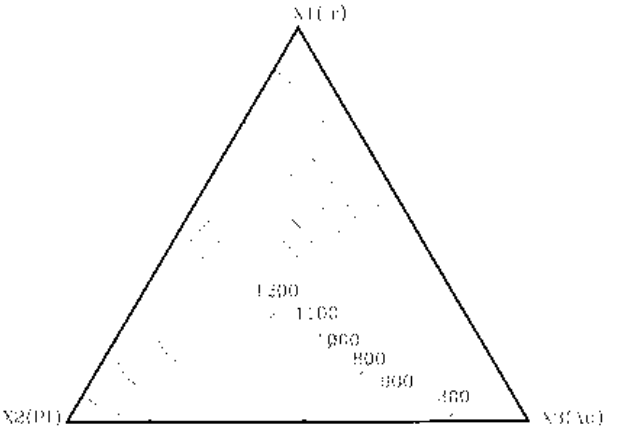

Fig. 6. A contour plot of apparent activity (μA cm^{-2}) for oxygen reduction against coating solution compositions for Ir–Pt–Au ternary oxide electrodes. Numbers associated with contour lines represent i results.

portional to the number of active sites, and current density is predominantly governed by both surface area and the specific activity of the electrocatalyst. The i/q^*, therefore, reveals the catalytic effects of mixed oxides in a unit of real surface area.

The regression equation for i/q^*, in Table 1, is of the following form:

$$\begin{aligned} i/q^* = {} & \underset{(1.50)}{15.48x_2} + \underset{(1.85)}{7.533x_3} + \underset{(7.80)}{47.56x_2x_3} - \underset{(6.98)}{10.17x_1x_3} \\ & + \underset{(59\,534.47)}{244\,631x_1x_2x_3} + \underset{(15.53)}{30.40x_1x_2(x_1 - x_2)} \\ & - \underset{(16.30)}{54.15x_2x_3(x_2 - x_3)} - \underset{(59\,561.97)}{244\,389x_1^2x_2x_3} \\ & - \underset{(59\,561.06)}{244\,454x_1x_2^2x_3} - \underset{59\,564.98)}{244506x_1x_2x_3^2} \end{aligned} \quad (3)$$

The analysis of variance indicates that the regression model is statistically significant. The surface and contour plots of electrocatalytic activity against Ir–Pt–Au ternary system is shown in Fig. 7. Note that the Pt–Au binary electrodes possess the maximum i/q^* value and that this value decreases with the increasing Ir contents in either binary (Ir–Pt, Ir–Au) or ternary (Ir–Pt–Au) systems. This result reflects the fact that the Pt–Au binary electrodes possess the higher specific activity for oxygen reduction than others.

The results of voltammetry charge (q^*) and surface morphology indicate that Pt 50%–Ir 50% binary electrode have a higher surface area than other electrodes. By maintaining the maximum q^* value, Ir–Pt binary electrodes demonstrate themselves as suitable substrate matrix for other materials. The better electrocatalytic activity in Pt 50%–Au 50% binary electrodes may be due to the efficient formation of hydrogen peroxide on Au in the first step of oxygen reduction [21–26], with platinum then accelerating the decomposition of hydrogen peroxide. Consequently, high active surface area coupled with the high electrocatalytic activity generated the maximum apparent oxygen reduction current observed in Ir–Pt–Au ternary electrodes. As discussed previously, Pt 50%–Ir 50% binary electrodes have the highest voltammetric charge and Pt 50%–Au 50% binary electrodes have the best electrocatalytic activity. On the basis of the combination of these two effects, the Ir 33%–Pt 33%–Au 33% ternary electrode is considered the most valuable cathode for oxygen reduction in alkaline media.

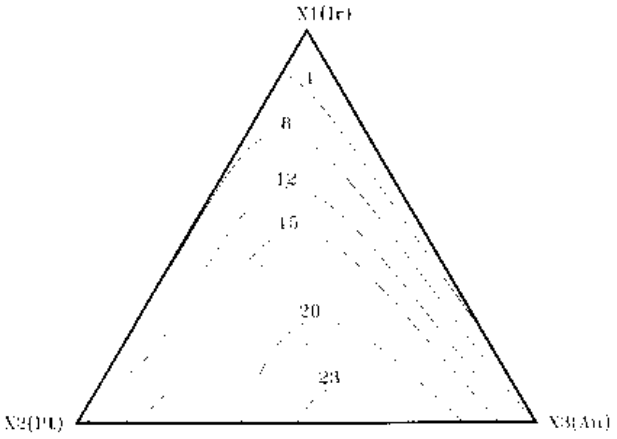

Fig. 7. A contour plot of electrocatalytic activity (μA mC^{-1}) against coating solution compositions for Ir–Pt–Au ternary oxide electrodes. Numbers associated with contour lines represent i/q^* results.

4. Conclusions

By means of statistical mixture experimental design, a regression model of the Ir–Pt–Au ternary electrode for oxygen reduction facilitates properties analysis. The coefficients of the regression models represented as contour plots were remarkably useful in studying the effects of coating solution composition as regards voltammetry charge, oxygen reduction, and electrocatalytic activity. The Pt 50%–Ir 50% binary electrode has the highest voltammetric charge and the Pt 50%–Au 50% binary electrode possesses the best electrocatalytic activity. Thus, the Ir 33%–Pt 33%–Au 33% ternary electrode is the best electrode for oxygen reduction in alkaline media.

Acknowledgement

Financial support of this work by the National Science Council of the Republic of China under contract NSC 86-2214-E006-007 and technical English consultation by Randy Gillespie are acknowledged.

References

[1] J. C. Huang, R. K. Sen and E. Yeager, *J Electrochem. Soc.* **126** (1979) 786.
[2] C. C. Wang, K. S. Goto and S. A. Akbar, *ibid.* **138** (1991) 3673.
[3] M. Sudoh, T. Kodera, H. Hino and H. Shimamura, *J. Chem. Eng. Japan* **21** (1988) 198.
[4] C. Oloman and A. P. Watkinson, *J. Appl. Electrochem.* **9** (1979) 117.
[5] E. Yeager, *Electrochim Acta* **29** (1984) 1527.
[6] S. Hackwood, W. C. Dautremont-Smith, G. Beni, L. M. Schiavone and J. L. Shay, *J. Electrochem. Soc.* **128** (1981) 1212.
[7] S. Trasatti (ed.), 'Electrodes of Conductive Metallic Oxides,' Parts A and B, Elsevier, Amsterdam (1980, 1981).
[8] S. M. Lin and T. C. Wen, *J. Electrochem. Soc.* **140** (1993) 2265.
[9] J. F. C. Boodts and S. Trasatti, *J. Appl. Electrochem.* **19** (1989) 255.
[10] H. Chen and S. Trasatti, *ibid.* **23** (1993) 559.
[11] L. D. Burke and D. P. Whelan, *J. Electroanal. Chem.* **162** (1984) 121.
[12] C. C. Chang and T. C. Wen, *J. Electrochem. Soc.* **143** (1996) 1473.
[13] B. C. Beard and P. N. Ross, Jr., *ibid.* **137** (1990) 3368.
[14] J. R. Anderson, 'Structure of Metallic Catalysts', Academic Press, New York (1975).
[15] N. R. K. Vilambi and E. J. Tayler, *Electrochim. Acta* **34** (1989) 1449.
[16] K. V. Ramesh, P. R. Sarode, S. Vasudevan and A. K. Shukla, *J. Electroanal. Chem.* **223** (1987) 91.
[17] D. S. Gnanamuthu and J. V. Petrocelli, *J. Electrochem. Soc.* **114** (1967) 1036.

[18] A. Damjanovic and V. Brusic, *J. Electroanal. Chem.* **15** (1967) 29.
[19] F. J. Luczak and D. A. Landsman, *US Patent 4 677 092* (1987).
[20] Y. Hayakawa, A. Kawashima, H. Habazaki, K. Asami, and K. Hashimoto, *J. Appl. Electrochem.* **22** (1992) 1017.
[21] A. Damjanovic, M. A. Genshaw and J. O'M. Bockris, *J. Electroanal. Chem.* **15** (1967) 173.
[22] B. G. Podliner and L. N. Nekrasov, *Sov. Electrochem.* **5** (1969) 308.
[23] H. S. Wroblowa, Y.-C. Pan and G. Razumney, *J. Electroanal. Chem.* **69** (1976) 195.
[24] R. W. Zurilla, R. K. Sen and E. Yeager, *J. Electrochem. Soc.* **125** (1978) 1103.
[25] P. Fischer and J. Heitbaum, *J. Electroanal. Chem.* **112** (1980) 231.
[26] R. R. Adzic, A. V. Tripkovic, N. M. Markovic, *ibid.* **114** (1970) 37.
[27] V. B. Baez and D. Pletcher, *ibid* **377** (1994) 231.
[28] Ch. Comninellis and G. P. Vercesi, *J. Appl. Electrochem.* **21** (1991) 335.
[29] T. A. F. Lassali, J. F. C. Boodts, S. C. de Castro, R. Landers and S. Trasatti, *Electrochim. Acta* **39** (1994) 95.
[30] M. Krausa, W. Vielstich, *J. Electroanal. Chem.* **379** (1994) 307.
[31] E. Gonzalez Hernan, C. Alonso, and J. Gonzalez-Velasco, *J. Appl. Electrochem.* **17** (1987) 868.
[32] R. Celdran and J. Gonzalez-Velasco, *Electrochim. Acta* **26** (1981) 525.
[33] P. Ocon, C. Alonso, R. Celdran and J. Gonzalez-Velasco, *J. Electroanal. Chem.* **206** (1986) 179.
[34] C. H. Bartholomew and Mbourdart, *J. Catal.* **29** (1973) 278.
[35] B. D. McNicol and R. T. Short, *J. Electroanal. Chem* **81** (1977) 249.
[36 S. Ardizzone, G. Fregonara, and S. Trasatti, *Electrochim. Acta* **35** (1990) 263.
[37] S. Trasatti, *ibid* **36** (1991) 225.
[38] S. M. Lin and T. C. Wen, *J. Appl. Electrochem.* **23** (1993) 487.
[39] J. A. Cornell, 'Experiments with Mixtures: Design, Models, and the Analysis of Mixture Data', 2nd edn., John Wiley & Sons, New York (1990).
[40] S. Trasatti, *Electrochim. Acta* **29** (1984) 1503.